JOURNAL OF AIRCRAFT
Vol. 48, No. 2, March–April 2011

Optimization of Helicopter Rotor Using Polynomial and Neural Network Metamodels

K. K. Saijal* and Ranjan Ganguli†
Indian Institute of Science, Bangalore 560012, India
and
S. R. Viswamurthy
National Aerospace Laboratories, Bangalore 560012, India

DOI: 10.2514/1.C031156

This study aims to determine optimal locations of dual trailing-edge flaps and blade stiffness to achieve minimum hub vibration levels in a helicopter, with low penalty in terms of required trailing-edge flap control power. An aeroelastic analysis based on finite elements in space and time is used in conjunction with an optimal control algorithm to determine the flap time history for vibration minimization. Using the aeroelastic analysis, it is found that the objective functions are highly nonlinear and polynomial response surface approximations cannot describe the objectives adequately. A neural network is then used for approximating the objective functions for optimization. Pareto-optimal points minimizing both helicopter vibration and flap power are obtained using the response surface and neural network metamodels. The two metamodels give useful improved designs resulting in about 27% reduction in hub vibration and about 45% reduction in flap power. However, the design obtained using response surface is less sensitive to small perturbations in the design variables.

Nomenclature

$\mathbf{C}$	=	finite element damping matrix
$\mathbf{F}$	=	finite element force vector
F_p	=	normalized measure of trailing-edge flap power
F_v	=	normalized measure of hub vibration level
GJ	=	blade torsional stiffness
GJ_{lower}, GJ_{upper}	=	move limits of torsional stiffness of blade
$\mathbf{J}$	=	quadratic cost functional
J_v^*	=	vibration cost functional due to optimal flap control input
$\mathbf{K}$	=	finite element stiffness matrix
$\mathbf{M}$	=	finite element mass matrix
M_h	=	trailing-edge flap hinge moment
N_b	=	number of blades
N_f	=	number of trailing-edge flaps in one rotor blade
P_t	=	total flap power; all blades combined
$\mathbf{q}$	=	blade global displacement vector
R	=	rotor radius
$\mathbf{W}_Z$	=	weighting matrix on vibration magnitude
$\mathbf{W}_\delta$	=	weighting matrix on control effort
x_1	=	inboard flap position
$x_{1\text{-lower}}$, $x_{1\text{-upper}}$	=	move limits for position of inboard flap
x_2	=	outboard flap position
$x_{2\text{-lower}}$, $x_{2\text{-upper}}$	=	move limits for position of outboard flap
$\mathbf{Z}$	=	vector of 4/rev hub loads
δ	=	trailing-edge flap deflection
$\delta_i^{2c}, \delta_i^{2s}, \ldots, \delta_i^{5c}, \delta_i^{5s}$	=	harmonics of trailing-edge flap motion
$\delta T, \delta U, \delta W$	=	virtual variation in kinetic energy, strain energy and virtual work
ψ	=	blade azimuth angle/nondimensional time
Ω	=	rotor rotational speed

Received 22 June 2010; accepted for publication 12 September 2010.

*Graduate Student, Department of Aerospace Engineering; saijal@aero.iisc.ernet.in.

†Professor, Department of Aerospace Engineering; ganguli@aero.iisc.ernet.in. Associate Fellow AIAA.

I. Introduction

HELICOPTERS are subjected to severe vibration levels compared with other flying vehicles because of the highly unsteady aerodynamic environment around the rotor and the flexibility of the long slender rotor blades [1]. The high vibration creates a hostile environment for the electronics and other equipment on board, making it difficult to read the instruments and leading to inaccurate weapon delivery. The impact of these high vibration levels on passenger and crew comfort is also critical. High vibration can also lead to fatigue in structural components and increased maintenance costs. Therefore, considerable efforts are made to reduce vibration levels in helicopters. The primary sources of vibration in the helicopter are main rotor system, the aerodynamic interaction between the rotor and the fuselage, the tail rotor, the engine and the transmission. The main rotor is the most significant source of vibration because of the highly unsteady aerodynamic environment acting on highly flexible rotating blades.

Dynamic vibration absorber and isolation mounting are the commonly used passive vibration control devices in a helicopter. These devices do not require any external power supply and they are usually easy to design and simple to implement. But the problem with these passive vibration control devices is that they are tuned for a particular cruise condition and cannot be changed once the rotor is in operation. Another drawback is the large weight penalty associated with these devices. The isolation system may cause large structural deflection during maneuver or transient flight condition. The dynamic pendulum absorbers mounted on the rotor blade may also add to the drag penalty of the helicopter [2].

Unfortunately, passive vibration control devices have not proved effective and efficient for the desired comfort level in rotorcraft flight. Therefore, researchers have turned towards the active vibration control approach in the past decade. There are mainly two subcategories in active vibration control: the airframe-based control and rotor-based control. In airframe-based control, the control actions are directly applied to the airframe so that the actuator-induced response will superimpose with the response due to the oscillatory hub loads canceling the vibration. The airframe-based

control approach has high weight penalty and the actuation system is highly complex leading to severe reliability and maintainability problems. Also, the vibration reduction capability is limited to airframe. higher harmonic control (HHC) is one of the rotor-based active control approaches in which vibration is suppressed at the source through excitation of the blade pitch at higher harmonics of the rotational speed. The HHC concept has been investigated through numerical simulations [3] and wind tunnel tests [4]. But the actuation system in this case is limited to N_b/rev excitation frequencies for an N_b bladed rotor. This can be resolved by the use of individual blade control (IBC) [5,6] in which each blade is individually controlled in the rotating frame over a wide range of desired frequencies. HHC and IBC have the potential for substantial vibration reduction, but both approaches have limitations in their practical implementations. Both of these methods have considerable weight penalties and high cost. Moreover, large actuation power is needed to pitch the entire blade and complex actuation system.

With the advancements in smart materials technology, especially piezoelectric materials, actively controlled trailing-edge flaps have been proposed as a low power localized actuator system to achieve IBC. In this method, one or more on-blade trailing-edge flaps, each of them spanning about 4–6% of the blade are actuated. This approach substantially reduces the control power for actuation when compared with HHC and IBC. Actively controlled trailing-edge flaps represent one of the most promising methods for vibration reduction in helicopters because of low power consumption, light weight, compact size, airworthiness and high adaptation. The potential of trailing-edge flap concept to reduce the vibratory hub loads, alleviate noise and enhance rotor performance has been demonstrated by several numerical [7,8] and experimental [9,10] investigations. Piezostack-based actuators are best suited for the actuation of trailing-edge flaps in full-scale rotor blades. Recent studies show that the multiple flaps are capable of achieving higher vibration reduction compared with single flap configuration within available actuator authority [11,12]. Multiple flaps provide more flexibility in altering the aerodynamic loads acting on the rotor blade as compared with a single trailing-edge flap.

Vibration reduction can also be achieved by better design of the rotor blade by tailoring structural, inertial and aerodynamic properties. Several research works have been done in the area of helicopter vibration reduction using structural and aeroelastic optimization [13–18]. The main focus of these studies was on reduction of rotor vibratory hub loads and enhancement of blade aeroelastic stability. Typically, the research addressed the problems of high vibration and low damped lag bending mode in the helicopter. The design variables in these studies are blade mass and elastic stiffness distributions, aerodynamic properties, composite ply angles and advanced blade geometry [19–23]. Reference [24] gives a review of helicopter rotor optimization.

Helicopter aeroelastic analysis are huge computer programs involving several disciplines and hence the integration of optimization algorithms with simulation codes is very cumbersome and time consuming. One approach to overcome this difficulty is to develop inexpensive surrogates or metamodels, which are function approximations to the expensive computer analysis. An excellent survey of metamodeling applications in engineering design including the most popular techniques like response surface methodology (RSM), kriging and neural network is given by Simpson et al. [25]. Metamodeling techniques have found wide use in structural and multidisciplinary design optimization [26,27]. Glaz et al. studied the effectiveness of surrogate-based optimization of helicopter rotor blades for vibration reduction at both low and high speed forward flight [28]. Bhadra and Ganguli [29] used orthogonal array-based metamodels for aeroelastic optimization of a helicopter rotor. In RSM, response surfaces approximations are created by sampled numerical experiments over the feasible design space. Usually the objectives and constraints are approximated using lower-order polynomial response surfaces. The method of least squares is used to determine the unknown regression coefficients in the response surfaces [30]. Once the response surfaces are obtained, it is easy to determine the optimum design variables because of the very low computational cost of evaluating polynomial functions. Response surface approximations have also found applications in reliability based design optimization problems [31,32]. Kriging is a regression technique originally used in geostatistics to approximate or interpolate data [33]. The accuracies of kriging, radial basis function interpolation, and polynomial regression surrogates in the optimization of helicopter rotor blades for vibration reduction are compared in [34]. Kriging models are capable of accurately approximating a highly nonlinear system by using fewer samples than RSM. However, kriging has found limited use in engineering design applications because of the high computational effort and difficulty in interpretation of model parameters. Comparative studies show that RSM is ideal for small-scale, mildly nonlinear problems [35]. Ganguli [36] used RSM for optimum design of helicopter rotor for low vibration taking the flap bending, lag bending and torsion stiffness as the design variables. The use of RSM in helicopter rotor optimization is again demonstrated by Viswamurthy and Ganguli [37] in their work on the optimum placement of dual trailing-edge flaps for low vibration with minimum flap control power. These studies show the potential of RSM to decouple the complicated aeroelastic analysis and optimization problems. However, there are situations where polynomial response surfaces do not yield adequate function approximations and more global methods such as neural networks need to be used.

Metamodeling using neural networks is best suited for highly nonlinear and very large problems [25]. A neural network is a massively parallel distributed processor made up of simple processing units called neurons, which has a natural capability to store knowledge and make it available for use. The network acquires knowledge from its environment through the learning process and uses interneuron connection strengths, known as synaptic weights to store the knowledge [38]. In a multilayer feedforward network, there are one or more hidden neuron layers which will intervene between the external input and the network output in some useful manner. Standard multilayer feedforward networks with as few as one hidden layer using appropriate hidden layer activation functions are capable of approximating any Borel measurable function from one finite dimensional space to another to any desired degree of accuracy, provided sufficient hidden layer neurons are available. A Borel measurable function is a real-valued function such that the inverse image of the set of real numbers greater than any given real number is a Borel set. In this sense, multilayer feedforward networks are a class of universal function approximators [39–42]. Linse and Stengel [43] used neural networks for function approximation in nonlinear control. Lee and Chen [44] developed a methodology with back-propagation neural network models to explore the artificial neural nets technology in design optimization. Specifying the architecture and training the network to perform well with reference to a training set are the two main issues in neural network applications. If the architecture is made large enough, a neural network can be a nearly universal approximator [45]. A review of the use of neural networks in structural analysis and design is given by Hajela and Berke [46]. Lee and Hajela [47] used neural networks for design optimization of rotor blades. In their work, a neural network based decomposition approach is proposed for partitioning the large-scale multidisciplinary design problem into smaller, more tractable subproblems.

A hybrid design method, combining trailing-edge flap controller design and blade structural optimization is proposed by Zhang et al. [48]. They used an integrated optimum control/structural optimization process to minimize the objective function, which includes vibratory hub loads and active flap control inputs for a helicopter rotor with a single trailing-edge flap. In this hybrid design study, for a given set of the passive design parameters, such as blade mass and stiffness distribution, the active control actions (i.e. active flap deflections) are predicted based on an optimal control law. The passive design parameters are then determined by a gradient-based nonlinear constrained minimization algorithm. Parallel computing is used to solve the rotor design optimization problem to integrate the active flap optimal control with the rotor structural optimization. The optimization package DOT is used in the optimization process.

In the present study, locations of dual trailing-edge flaps and blade elastic stiffnesses are the design variables with the objective of vibration reduction with minimum flap control power. A parametric study showed that flap bending and lag bending stiffnesses do not contribute significantly to the objectives and are hence omitted from the design variables. An aeroelastic analysis showed that the introduction of torsional stiffness as a design variable along with location of dual trailing-edge flaps makes the objective functions highly nonlinear and polynomial response functions are unable to approximate them adequately. So this study uses the neural networks as a metamodeling technique to approximate the objective functions because neural network is well suited for approximating highly nonlinear functions.

II. Helicopter Aeroelastic Analysis

The helicopter is represented as a nonlinear model of several elastic rotor blades dynamically coupled to a rigid fuselage. Each rotor blade undergoes moderate displacement and small strain in flap, lag and torsion. The system equation of motion is derived using Hamilton's variational principle:

$$\delta\Pi = \int_{\psi_1}^{\psi_2} (\delta U - \delta T - \delta W)\, \mathrm{d}\psi = 0 \tag{1}$$

where δU, δT and δW are virtual variations of strain energy, kinetic energy and virtual work done by external force, respectively, and $\delta\Pi$ represents the total potential of the system. The aerodynamic loads in the rotor blade with trailing-edge flaps are calculated using unsteady aerodynamic models [49,50] and a reverse flow model [51].

Finite element method is used to convert the nonlinear, coupled, partial differential equations obtained from Eq. (1) to nonlinear, coupled ordinary differential equations. In a discretized rotor blade, Hermite polynomials are used as shape functions for in-plane and out-of-plane bending and Lagrange polynomials for axial and torsion deflections. Using finite element method, it is easy to model nonuniform mass and stiffness properties of the helicopter blade along the span. The global mass, damping, stiffness matrices and force vector are obtained by assembling the element mass, damping, stiffness matrices and force vector, respectively. Applying boundary conditions, Eq. (1) becomes

$$\mathbf{M}\,\ddot{\mathbf{q}}(\psi) + \mathbf{C}\dot{\mathbf{q}}(\psi) + \mathbf{K}\mathbf{q}(\psi) - \mathbf{F}(\mathbf{q}, \ddot{\mathbf{q}}, \psi) = \mathbf{0} \tag{2}$$

In the preceding equation, nonlinear terms are moved into the force vector, $\mathbf{F}$ and the equation is transformed to the modal co-ordinates using normal mode transformation. Only first ten modes are used for the aeroelastic analysis removing the higher natural modes by truncation, which reduces the number of differential equations to be solved and increases the efficiency of analysis. The ten nonlinear ordinary differential equations are then solved for the blade steady-state response using finite element in time method and Newton–Raphson procedure. The normal mode coordinates inside the time elements are approximated using mixed Lagrange–Hermite polynomials as shape functions. This allows the enforcement of continuity of generalized displacements and velocities within the time elements. The coupled trim/aeroelastic solution procedure is used to solve the blade response, pilot trim control angles and helicopter orientation simultaneously [36].

The fixed frame hub loads are calculated by summing the contributions of individual blades at the root after obtaining the steady-state blade response. $N_b\Omega$ harmonic is the dominant component of hub vibratory loads for an N_b bladed helicopter rotor with identical blades. This $N_b\Omega$ component of hub loads which are also called N_b per revolution loads or simply N_b/rev loads is the main source of vibration transmitted to the airframe. The focus of this study is to minimize the N_b/rev loads propagated to the airframe by optimal placement of two trailing-edge flaps along with optimum stiffnesses of the rotor blade (Fig. 1).

III. Flap Control Algorithm

The control approach is formulated in frequency-domain instead of time-domain [52] because the rotor loading and blade response are periodic in time under steady flight conditions. In a four-bladed rotor, the flaps are deflected at 2, 3, 4 and 5/rev harmonics of the rotor rotational speed. The trailing-edge flap motion is properly phased to cancel out the original vibratory loads at the rotor hub with new unsteady aerodynamic loads generated due to flap motion. The control law for the ith flap can be written as

$$\begin{aligned}\delta_i(\psi) = {} & \delta_i^{2c}\cos(2\psi) + \delta_i^{2s}\sin(2\psi) + \delta_i^{3c}\cos(3\psi) + \delta_i^{3s}\sin(3\psi) \\ & + \delta_i^{4c}\cos(4\psi) + \delta_i^{4s}\sin(4\psi) + \delta_i^{5c}\cos(5\psi) + \delta_i^{5s}\sin(5\psi)\end{aligned} \tag{3}$$

Each flap motion is defined by eight independent variables called flap harmonics which are determined based on optimality criterion. The control algorithm is based on the minimization of quadratic objective function

$$J = \mathbf{Z}^T\mathbf{W}_Z\mathbf{Z} + \delta^T\mathbf{W}_\delta\delta \tag{4}$$

where $\mathbf{Z}$ is the hub vibratory load vector containing N_b/rev sine and cosine harmonics; δ is the active flap control input vector containing cosine and sine higher harmonics; W_z and W_δ are the weighting matrices for vibration and control effort, respectively. In this study, the weighting matrix W_δ is adjusted to limit the peak deflection of both flaps to ± 2 degrees which can be achieved using current state-of-art smart materials. The hub forces and moments are non-dimensionalized with respect to $m_0\Omega^2R^2$ and $m_0\Omega^2R^3$, respectively. In the current study, all hub shears and moments are weighted equally. A global controller is used to determine the optimal control input. The first order Taylor series expansion about the zero control input (no trailing-edge flap motion) is evaluated:

$$\mathbf{Z} = \mathbf{Z}_0 + \mathbf{T}_0\delta \tag{5}$$

$\mathbf{T}_0$ is a gradient transfer matrix which relates the sine and cosine amplitudes of the control harmonics to the sine and cosine amplitudes of the vibration harmonics. It is assumed to be constant over the entire range of the control input and thus numerically computed only once by perturbing the control harmonics individually around zero control inputs using the forward difference method. Equation (5) is substituted into Eq. (4) and the following optimality condition is applied:

$$\frac{\partial J}{\partial \delta} = \mathbf{0} \tag{6}$$

Then the optimal controller becomes

$$\delta^* = \mathbf{C}\mathbf{Z}_0 \tag{7}$$

where

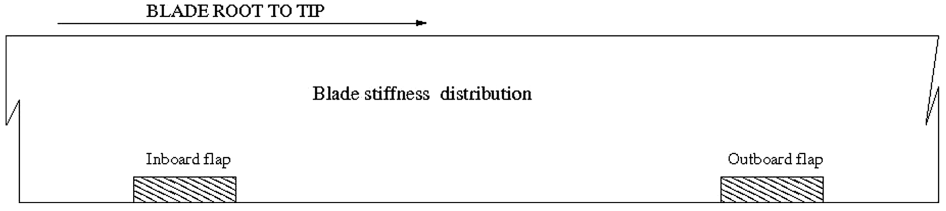

Fig. 1 Rotor with two trailing-edge flaps.

$$\mathbf{C} = -\mathbf{D}\mathbf{T}_0^T\mathbf{W}_Z \tag{8}$$

$$\mathbf{D} = (\mathbf{T}_0^T\mathbf{W}_Z\mathbf{T}_0 + \mathbf{W}_\delta)^{-1} \tag{9}$$

This controller is an open-loop strategy, wherein the optimal control input is determined purely based on the uncontrolled N_b/rev hub loads. The vibration level at the hub due to optimal control input is denoted by J_v^*:

$$J_v^* = \mathbf{Z}^{*T}\mathbf{Z}^* \tag{10}$$

The mean power required by a trailing-edge flap is obtained by integrating the product of the flap hinge moment and flap deflection rate over one complete rotor revolution:

$$P = -\frac{1}{2\pi}\int_0^{2\pi} M_h \frac{\mathrm{d}\delta}{\mathrm{d}\psi}\,\mathrm{d}\psi \tag{11}$$

The flap power changes sign over some portions of the azimuth and actuation mechanism will generally not be able to transfer this power back to the flap actuation power supply and hence the negative power is neglected. Then, the mean actuation power will be

$$P = \frac{1}{2\pi}\int_0^{2\pi} \max\left(-M_h \frac{\mathrm{d}\delta}{\mathrm{d}\psi}, 0\right)\mathrm{d}\psi \tag{12}$$

The mean actuation power for the complete flap system for a N_b bladed rotor with N_f flaps in each rotor blade can be written as

$$P_t = \frac{N_b}{2\pi}\sum_{i=1}^{N_f}\int_0^{2\pi} \max\left(-M_h \frac{\mathrm{d}\delta}{\mathrm{d}\psi}, 0\right)\mathrm{d}\psi \tag{13}$$

The values of J_v^* and P_t are normalized with respect to their baseline values. These normalized values are denoted by F_v and F_p, respectively.

IV. Response Surface Methodology

RSM is a collection of mathematical and statistical techniques that are useful for modeling problems [29]. Typically, response surfaces are smooth analytical functions that are approximated by low-order polynomials. The approximations can be expressed as

$$y(x) = f(x) + \epsilon \tag{14}$$

where $y(x)$ is the unknown function of interest, $f(x)$ is a known polynomial function of x, and ϵ is random error. If the response is modeled by a nonlinear function of k independent variables, then the approximating function is the second order model given by

$$y = \beta_0 + \sum_{i=1}^{k}\beta_i x_i + \sum_{i=1}^{k}\beta_{ii}x_i^2 + \sum\sum_{i<j}\beta_{ij}x_i x_j + \epsilon \tag{15}$$

The unknown regression coefficients β_0, β_i, β_{ii} and β_{ij} of the polynomial in Eq. (15) are determined through least-squares regression, which minimizes the sum of the squares of the deviations of predicted values, $\hat{y}(x)$, from the actual values, $y(x)$. To evaluate the unknown parameters, Eq. (15) can be written as

$$y = X\beta + \epsilon \tag{16}$$

where y is a $n \times 1$ vector of responses and X is a $n \times p$ matrix of sample data points given as

$$X = \begin{bmatrix} 1 & x_{11} & x_{12} & x_{11}^2 & x_{12}^2 & x_{11}x_{12} \\ 1 & x_{21} & x_{22} & x_{21}^2 & x_{22}^2 & x_{21}x_{22} \\ . & . & . & . & . & . \\ . & . & . & . & . & . \\ 1 & x_{n1} & x_{n2} & x_{n1}^2 & x_{n2}^2 & x_{n1}x_{n2} \end{bmatrix} \tag{17}$$

and β is a $p \times 1$ vector of the regression parameters, ϵ is a $p \times 1$ vector of error terms, and p is the number of design points. The parameters β_0, β_i, β_{ii} and β_{ij} are obtained by minimizing the least-square error using Eq. (16) [30]:

$$L = \sum_{i=1}^{n}\epsilon_i^2 = \epsilon^T\epsilon = (y - X\beta)^T(y - X\beta) \tag{18}$$

which gives

$$L = y^T y - 2\beta^T X^T y + \beta^T X^T X\beta \tag{19}$$

where L is the square of the error. Equation (19) is differentiated with respect to β to minimize L:

$$\left.\frac{\partial L}{\partial \beta}\right|_{\hat{\beta}} = -2X^T y + 2X^T X\hat{\beta} = 0 \tag{20}$$

or

$$\hat{\beta} = (X^T X)^{-1}X^T y \tag{21}$$

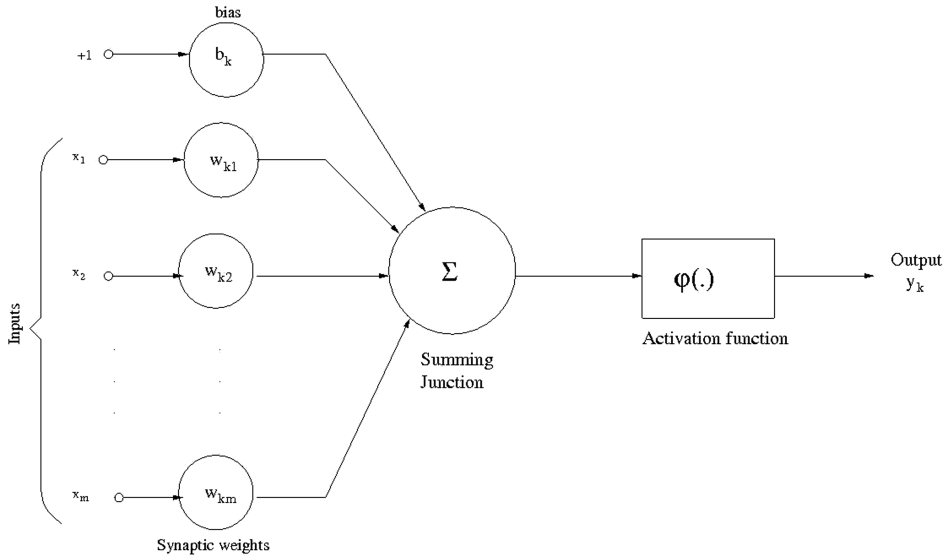

Fig. 2 Nonlinear model of neuron.

Therefore, the fitted regression model is

$$\hat{y} = X\hat{\beta} \tag{22}$$

V. Neural Networks

A neural network is a massively parallel distributed processor made up of simple processing units called neurons [38]. Three basic elements of the neuronal model are a set of synapses or connecting links, each of which is characterized by a weight or strength of its own, an adder for summing the input signals weighted by the respective synapses of the neuron and an activation function for limiting the amplitude of the output of a neuron (Fig. 2). The neuron model also includes an externally applied bias, denoted by b_k which increases or decreases the net input of the activation function, depending on whether it is positive or negative, respectively. A neural network made up of an interconnection of nonlinear neurons is also nonlinear. Nonlinearity which is distributed throughout the network is a highly important property of the neural network. In the learning process, the synaptic weights of the network are modified to minimize the difference between the desired response and the actual response of the network produced by the input signal in accordance with an appropriate statistical criterion.

Mathematically, a neuron k can be described by the following equations:

$$u_k = \sum_{j=1}^{m} w_{kj} x_j \tag{23}$$

and

$$y_k = \varphi(u_k + b_k) \tag{24}$$

where $x_1, x_2, \ldots, x_m$ are the inputs; $w_{k1}, w_{k2}, \ldots, w_{km}$ are the synaptic weights of neuron k; u_k is the linear combiner output due to the inputs; b_k is the bias; $\varphi(.)$ is the activation function; and y_k is the output of the neuron. The activation function can be chosen as the threshold function, piecewise-linear function or sigmoid function depending on the applications.

In a layered neural network, the neurons are organized in the form of layers. A multilayer feedforward network consists of an input layer, one or more hidden layers, and an output layer in which computations take place in the hidden and output layers only. The input signal propagates through the network in a forward direction, layer-by-layer. Multilayer perceptron networks are typically trained using error back-propagation algorithm. Learning consists of two passes through the different layers of a MLP network. In the forward pass, the output (response) of the network to an input vector is computed keeping all the synaptic weights fixed. During the backward pass, the error signal is propagated backward through the network and the weights are adjusted using an error-correction rule. After adjustment, the output of the network should have moved closer to the desired response in a statistical sense. The main features of a multilayer perceptron network are the neurons modeled with a smooth nonlinear activation function, hidden layer(s) and high degree of connectivity which gives high computational power for the network (Fig. 3).

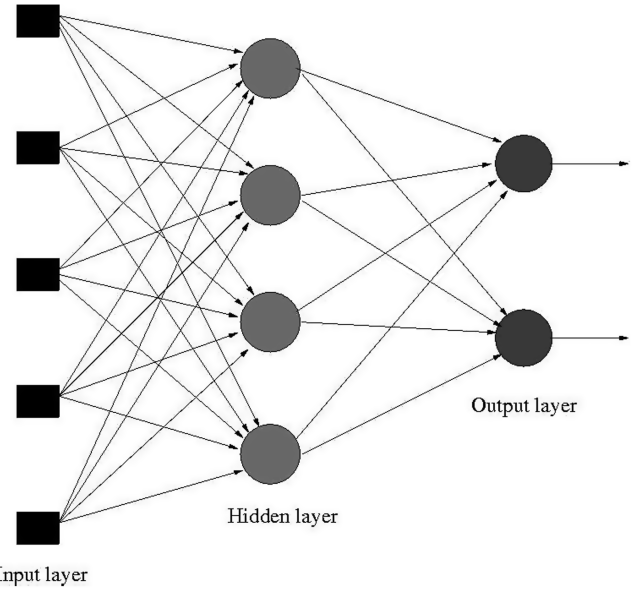

Fig. 3 Fully connected feedforward network with one hidden layer and one output layer.

In the present study, a feedforward back-propagation network with a single hidden layer is used. The hidden layer uses the hyperbolic tangent sigmoid transfer function. The output layer uses a linear transfer function. This network uses Levenberg–Marquardt back-propagation training function which updates the weights and bias values according to Levenberg–Marquardt optimization, a gradient descent with momentum weight and bias back-propagation learning function and mean squared error performance function in which the performance is measured according to the mean of squared errors.

VI. Parametric Study

The objective of the present study is to reduce hub vibration and control power for the flaps by placing the flaps at the optimal location with optimal stiffnesses of the rotor blade. The design variables in this study are the locations of the two trailing-edge flaps and stiffnesses of the rotor blade. A parametric study is conducted by varying the design variables one at a time while keeping the others fixed at the baseline value. The results of parametric study are shown in Fig. 4 which shows that the variations in locations of trailing-edge flaps and torsional stiffness of the rotor blade contribute favorably to the objectives considered (Figs. 4a, 4b, and 4e). The variations in flap and lag bending stiffness of the rotor blade have very little favorable effect on the objectives of the problem and are hence removed from the design variables (Figs. 4c and 4d). The torsional stiffness has significant favorable effect and is used as the structural design variable.

VII. Optimization Problem

The present study aims to find the optimal locations of the trailing-edge flaps and the torsional stiffness of the rotor blade to achieve maximum reduction in hub vibration, F_v, with minimum penalty in terms of trailing-edge flap actuation power, F_p, consumed by the active flap system. The design variables considered for this study are the inboard flap position, x_1, outboard flap position, x_2 and normalized blade torsional stiffness, GJ. Upper and lower bounds (move limits) are imposed on the design variables. The numerical values for initial configuration and move limits for variables x_1, x_2 and GJ are given in Table 1. The inboard and outboard flaps are constrained to be placed between 59 to 71 and 77 to 89% blade span, respectively, so that the midpoint of each flap can move one flap span length (i.e. 6% of blade span) to the left or right. The lower limit on the inboard flap prevents it from operating in a comparatively low dynamic pressure region. The upper limit on the outboard flap prevents it from being placed too near the blade tip since the flow there is three-dimensional in nature and is dominated by strong tip vortices whose effect on the flap cannot be modeled using two dimensional aerodynamic models. The lower and upper bounds of torsional stiffness is selected at 25% lower and greater than the baseline design, respectively. The upper bound on the stiffness acts as an implicit constraint on-blade frequencies and dynamic stresses and the lower bound acts as a constraint on-blade deflections. The optimization problem can be posed as

$$\text{Minimize } \{F_v, F_p\} \qquad \text{Subject to: } x_{1\text{-lower}} \le x_1 \le x_{1\text{-upper}}$$

$$x_{2\text{-lower}} \le x_2 \le x_{2\text{-upper}} \qquad GJ_{\text{lower}} \le GJ \le GJ_{\text{upper}}$$

This is a multi-objective optimization problem with constraints. The nature of the trade off between the two objectives depends on the

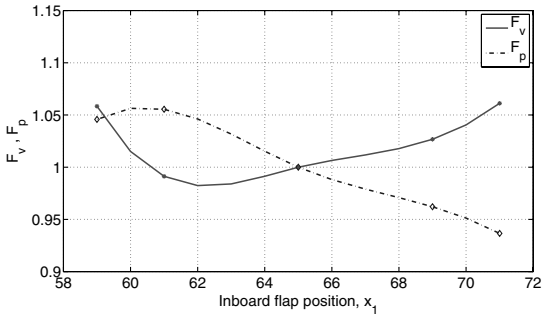

a) With inboard flap position, x_1

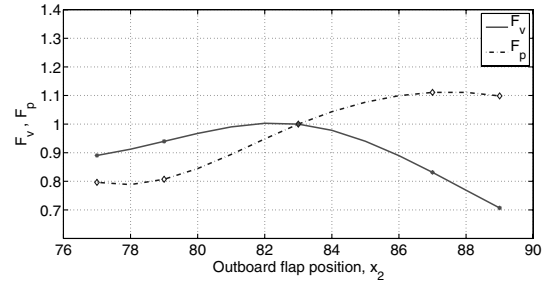

b) With outboard flap position, x_2

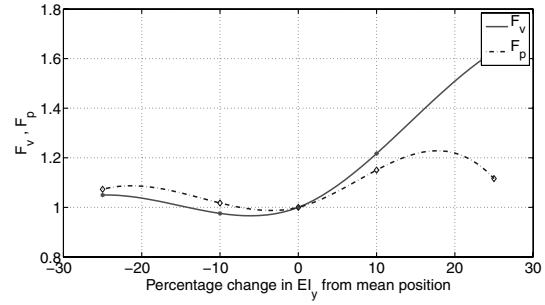

c) With flap stiffness, EI_y

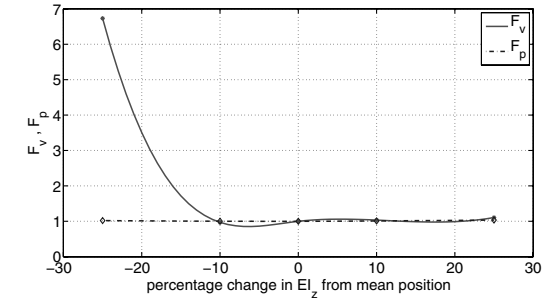

d) With lag stiffness, EI_z

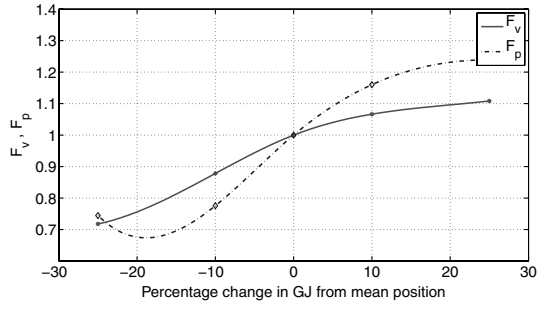

e) With torsional stiffness, GJ

Fig. 4 Variation of hub vibration, F_v and trailing-edge flap power, F_p with one design variable varied and others kept at baseline values.

Table 1 Initial configuration and move limits

Design variable	Lower limit	Baseline value	Upper limit
x_1	$0.59R$	$0.65R$	$0.71R$
x_2	$0.77R$	$0.83R$	$0.89R$
GJ	0.00461	0.00615	0.00769

shape of Pareto curve/surface. A solution is said to be Pareto-optimal if it is impossible to minimize any one objective without allowing an increase in one or more of the other objectives.

VIII. Numerical Results

Numerical results are obtained for a four-bladed, soft in-plane, uniform hingeless rotor similar to the BO105 rotor with twin trailing-edge flaps whose properties are given in Table 2. The trailing-edge flaps considered in this study are plain flaps where the flap is integrated into the airfoil cross-section. Span of each flap is 6% of blade span. The study is conducted at the cruise speed corresponding to an advance ratio of $\mu = 0.30$ using an aeroelastic analysis based on finite elements in space and time [51]. A coupled trim procedure is used for solving the rotor blade response and trim equations simultaneously.

A. Response Surface Generation

Using the helicopter aeroelastic analysis, the two objective functions F_v and F_p are evaluated at the data points corresponding to central composite design (CCD) with subscaled 2^k for three variables. The response surfaces are obtained by minimizing the error square [30] as

$$F_v = 0.9832 + 0.0125x_1 - 0.0650x_2 + 0.1074GJ + 0.0191x_1^2 - 0.0680x_2^2 - 0.0298GJ^2 - 0.0072x_1x_2 + 0.0110x_1GJ - 0.0680x_2GJ \quad (25)$$

$$F_p = 0.9471 - 0.0183x_1 + 0.2584x_2 + 0.0346GJ + 0.0303x_1^2 + 0.0151x_2^2 + 0.0304GJ^2 + 0.0294x_1x_2 - 0.0245x_1GJ - 0.1466x_2GJ \quad (26)$$

The comparison of response surface prediction and aeroelastic analysis at the CCD with subscaled 2^k data points for the objectives F_v and F_p are shown in Tables 3 and 4, respectively.

The error in response surface approximation of the objective function F_v is less than 6% but for the objective function F_p, it is as high as 31%. So it is clear that the response surface generated is not

Table 2 Rotor blade and trailing-edge flap properties

Properties	Value
Rotor	
N_b	4
c/R	0.055
Solidity, σ	0.07
Lock number, γ	5.20
C_T/σ	0.07
Blade pretwist	0.0
Precone, β_p	0.0
$EI_y/m_0\Omega^2R^4$	0.0108
$EI_z/m_0\Omega^2R^4$	0.0268
$GJ/m_0\Omega^2R^4$	0.00615
m_0, kg/m,	6.46
Ω, rpm,	383
R, m	4.94
Trailing-edge flap	
c_f/c	0.20
m_f/m_0	0.10
X_g/c_f	0.20

Table 3 Comparison of response surface, aeroelastic analysis and neural network predictions of F_v at data points

	Coded value			Physical variable			Hub vibration, F_v			Percent error	
S. No.	x_1	x_2	GJ	x_1	x_2	GJ	RSM prediction	Analysis prediction	Neural network	RSM	Neural network
1	0	0	0	0.65R	0.83R	0.00615	0.9832	1.0000	1.0073	−1.68	0.73
2	1	−1	−1	0.68R	0.80R	0.00526	0.8028	0.8277	0.8204	−3.00	−0.89
3	1	1	1	0.68R	0.86R	0.00704	0.8953	0.8984	0.9236	−0.34	2.81
4	1	−1	1	0.68R	0.80R	0.00704	1.1757	1.1535	1.1356	1.92	−1.55
5	1	1	−1	0.68R	0.86R	0.00526	0.7946	0.7823	0.8046	1.57	2.85
6	−1	1	1	0.62R	0.86R	0.00704	0.8627	0.8147	0.8595	5.89	5.50
7	−1	−1	1	0.62R	0.80R	0.00704	1.1143	1.1017	1.1448	1.14	3.91
8	−1	−1	−1	0.62R	0.80R	0.00526	0.7854	0.7658	0.7998	2.56	4.44
9	−1	1	−1	0.62R	0.86R	0.00526	0.8059	0.7829	0.7883	2.94	0.68
10	1.732	0	0	0.71R	0.83R	0.00615	1.0623	1.0612	1.0320	0.10	−2.75
11	−1.732	0	0	0.59R	0.83R	0.00615	1.0189	1.0584	1.0698	−3.73	1.07
12	0	1.732	0	0.65R	0.89R	0.00615	0.6669	0.7069	0.6625	−5.66	−6.29
13	0	−1.732	0	0.65R	0.77R	0.00615	0.8919	0.8903	0.8339	0.18	−6.33
14	0	0	1.732	0.65R	0.83R	0.00769	1.0798	1.1083	1.0926	−2.57	−1.42
15	0	0	−1.732	0.65R	0.83R	0.00461	0.7078	0.7177	0.7319	−1.38	1.97
16	0.5	0.5	0.5	0.67R	0.85R	0.00659	0.9750	0.9482	0.9703	2.83	2.33
17	0.5	0.5	−0.5	0.67R	0.85R	0.00571	0.8961	0.8665	0.8882	3.42	2.50
18	0.5	−0.5	0.5	0.67R	0.81R	0.00659	1.0776	1.1081	1.0791	−2.76	−2.61
19	0.5	−0.5	−0.5	0.67R	0.81R	0.00571	0.9307	0.9190	0.9045	1.26	−1.58
20	−0.5	0.5	0.5	0.63R	0.85R	0.00659	0.9606	0.9494	0.9234	1.18	−2.74
21	−0.5	0.5	−0.5	0.63R	0.85R	0.00571	0.8927	0.9275	0.8517	−3.76	−8.17
22	−0.5	−0.5	0.5	0.63R	0.81R	0.00659	1.0560	1.0697	1.0837	−1.28	1.31
23	−0.5	−0.5	−0.5	0.63R	0.81R	0.00571	0.9200	0.8978	0.8677	2.48	−3.35

able to approximate the actual objectives adequately. Addition of more points and use of higher order polynomials are not able to resolve this problem due to the localized nature of the nonlinearity. Therefore, we next use the neural network for this approximation problem.

B. Neural Network

Figures 5–10 shows a comparison of response surface method and neural network with actual aeroelastic analysis for the objectives F_v and F_p, respectively. These results are plotted by varying two of the design variables at a time, keeping the third one fixed at the baseline value. For aeroelastic analysis, each of the design variable is discretized into five points equally spaced within the move limits. Spline interpolation is used to get the intermediate values to draw the plots. From the plots of this actual analysis, it is clear that the objectives are highly nonlinear functions, especially the trailing-edge flap power, F_p. Figures 5–10 also show that the response surface functions are not able to adequately capture the details of local nonlinearity present in the objective functions. But the neural network is able to approximate the objectives fairly well compared with the response surface. A comparison of neural network prediction and aeroelastic analysis at the CCD with subscaled 2^k data points for the objectives F_v and F_p are also shown in Tables 3 and 4, respectively. There is a clear improvement in the prediction of F_p by using the neural network metamodel as seen in Table 4. Number of hidden layer neurons are 20 and 15 in F_v and F_p network, respectively. Number of neurons used in the hidden layer of the network is optimized to get minimum error at the CCD with subscaled 2^k data points.

Even though the neural network approximate the objectives fairly well compared with response surface, the plots obtained using neural

Table 4 Comparison of response surface, aeroelastic analysis and neural network predictions of F_p at data points

	Coded value			Physical variable			Flap power, F_p			% error	
S. No.	x_1	x_2	GJ	x_1	x_2	GJ	RSM prediction	Analysis prediction	Neural network	RSM	Neural network
1	0	0	0	0.65R	0.83R	0.00615	0.9471	1.0000	0.9426	−5.23	−5.74
2	1	−1	−1	0.68R	0.80R	0.00526	0.5601	0.5570	0.5769	0.56	3.58
3	1	1	1	0.68R	0.86R	0.00704	1.1559	1.1655	1.1494	−0.83	−1.39
4	1	−1	1	0.68R	0.80R	0.00704	0.8734	0.7415	0.8105	17.79	9.30
5	1	1	−1	0.68R	0.86R	0.00526	1.4290	1.7685	1.3370	−19.19	−24.40
6	−1	1	1	0.62R	0.86R	0.00704	1.1829	1.2333	1.1046	−4.09	−10.44
7	−1	−1	1	0.62R	0.80R	0.00704	1.0180	0.7878	0.9070	29.22	15.13
8	−1	−1	−1	0.62R	0.80R	0.00526	0.6065	0.6428	0.7484	−5.64	16.43
9	−1	1	−1	0.62R	0.86R	0.00526	1.3579	1.5863	1.4117	−14.40	−11.01
10	1.732	0	0	0.71R	0.83R	0.00615	1.0063	0.9366	0.8170	7.44	−12.76
11	−1.732	0	0	0.59R	0.83R	0.00615	1.0699	1.0458	0.9083	2.30	−13.14
12	0	1.732	0	0.65R	0.89R	0.00615	1.4400	1.0986	1.1134	31.08	1.35
13	0	−1.732	0	0.65R	0.77R	0.00615	0.5448	0.7924	0.7889	−31.25	−0.44
14	0	0	1.732	0.65R	0.83R	0.00769	1.0983	1.2386	1.1091	−11.33	−10.46
15	0	0	−1.732	0.65R	0.83R	0.00461	0.9786	0.7445	0.7546	31.44	1.36
16	0.5	0.5	0.5	0.67R	0.85R	0.00659	1.0680	1.1840	1.0824	−9.80	−8.59
17	0.5	0.5	−0.5	0.67R	0.85R	0.00571	1.1190	0.9806	1.0750	14.11	9.63
18	0.5	−0.5	0.5	0.67R	0.81R	0.00659	0.8681	0.8510	0.8915	2.02	4.76
19	0.5	−0.5	−0.5	0.67R	0.81R	0.00571	0.7725	0.7267	0.7808	6.31	7.44
20	−0.5	0.5	0.5	0.63R	0.85R	0.00659	1.0839	1.2218	1.0877	−11.29	−10.98
21	−0.5	0.5	−0.5	0.63R	0.85R	0.00571	1.1104	1.0229	1.0654	8.55	4.15
22	−0.5	−0.5	0.5	0.63R	0.81R	0.00659	0.9135	0.8961	0.9785	1.94	9.19
23	−0.5	−0.5	−0.5	0.63R	0.81R	0.00571	0.7933	0.7751	0.6861	2.35	−11.49

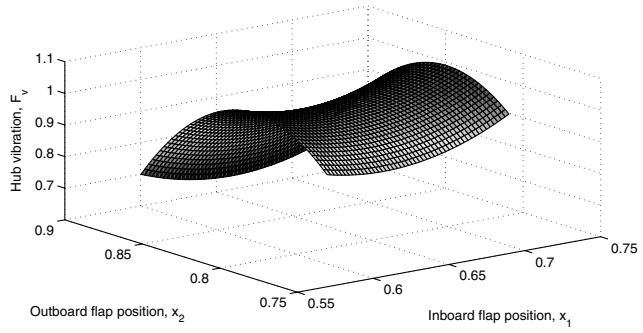

a) Response surface method

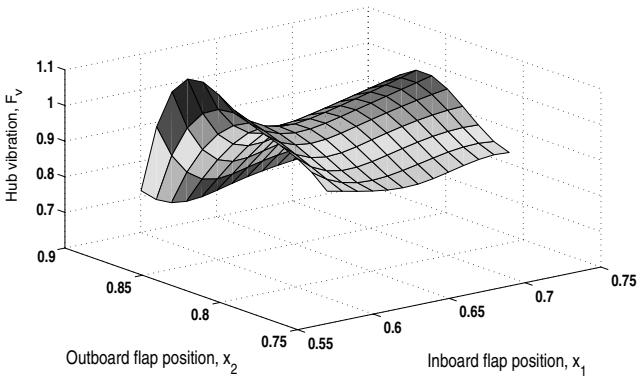

b) Aerelastic analysis

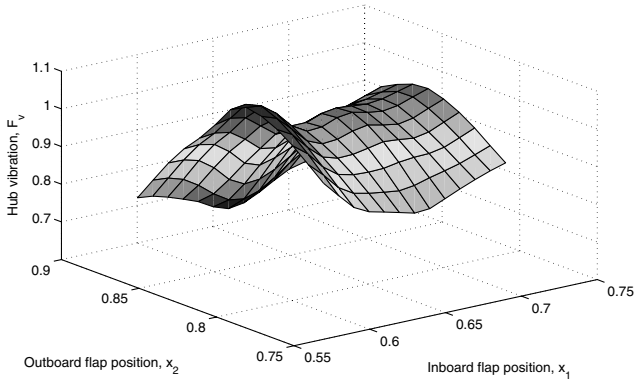

c) Neural network

Fig. 5 Variation in hub vibration, F_v, with respect to inboard flap position, x_1, and outboard flap position, x_2, with torsional stiffness, GJ, held constant at baseline value.

network shows slight differences from that of the actual analysis, especially the plots of F_p (Figs. 8–10). This may be due to the errors in neural network approximation, which is more in F_p compared with F_v, as given in Tables 3 and 4. The discretization of flap location design variable to get the actual analysis plots may also cause this difference.

C. Optimization Results

1. *Response Surface Method*

Single objective optimization: firstly, a single objective optimization is conducted using the response surface functions. An exhaustive search conducted in the design space using the F_v response surface with the objective of minimizing the hub vibration gives an optimal value of design variable as $x_1 = 0.64R$, $x_2 = 0.77R$ and $GJ = 0.00461$. An actual aeroelastic analysis at this optimal point gives $F_v = 0.7233$ and $F_p = 0.5755$. This is about 28% reduction in F_v and 42% reduction in F_p. Similarly, an exhaustive search with the objective of minimizing flap power alone gives an optimum design point as $x_1 = 0.67R$, $x_2 = 0.77R$ and $GJ = 0.00461$. Actual aeroelastic analysis at this point gives $F_v = 0.7864$ and $F_p = 0.9005$. This is about 21% reduction in F_v and only about 10% reduction in F_p. The single objective optimization with the objective of minimizing flap power alone gives lesser reduction in F_p compared with the single objective optimization with the objective of minimizing hub vibration alone. This anomalous result occurs because the response surface for F_p is not good enough to approximate the actual flap power objective. However, usable designs are obtained even with the poorly fitted polynomial response surfaces.

Multi-objective optimization: Fig. 11 shows the hub vibration levels and trailing-edge flap power resulting from various design choices within the move limits. It is obtained by moving from design space (x_1, x_2, GJ) to criterion space (F_v, F_p) using response surface metamodel. The design point $F_v = F_p = 1$ corresponds to the initial design point (baseline value). The Pareto-optimal front minimizing both hub vibration and flap power is only a point marked as A in

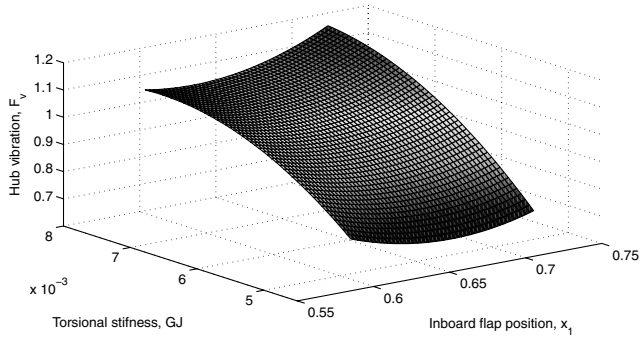

a) Response surface method

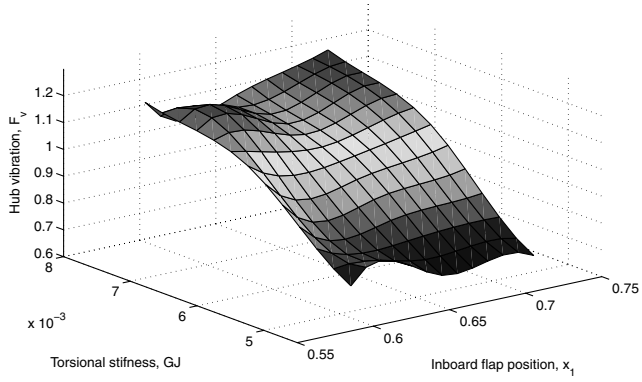

b) Aeroelastic analysis

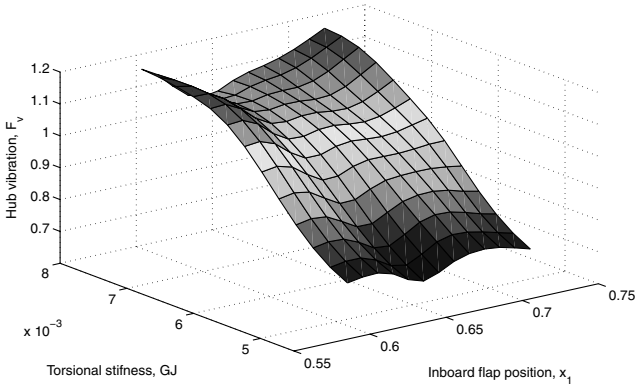

c) Neural network

Fig. 6 Variation in hub vibration, F_v, with respect to inboard flap position, x_1, and torsional stiffness, GJ, with outboard flap position, x_2, held constant at baseline value.

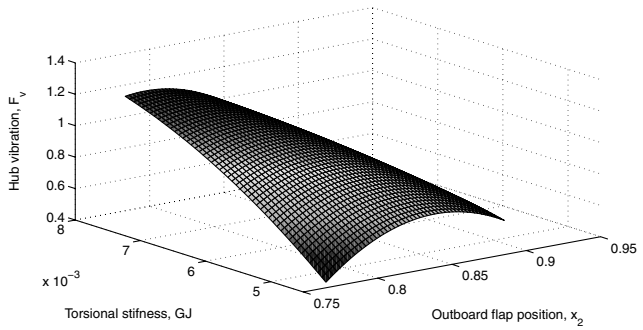

a) Response surface method

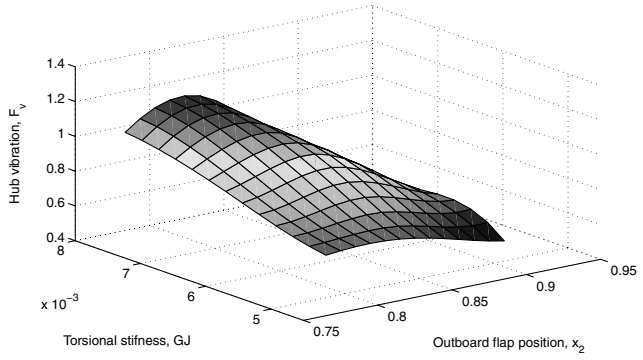

b) Aeroelastic analysis

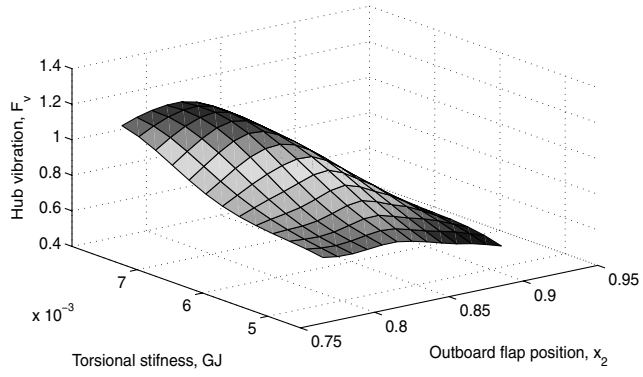

c) Neural network

Fig. 7 Variation in hub vibration, F_v, with respect to outboard flap position, x_2, and torsional stiffness, GJ, with inboard flap position, x_1, held constant at baseline value.

Fig. 11. The design point A corresponds to design variables $x_1 = 0.65R$, $x_2 = 0.77R$ and $GJ = 0.00461$. Aeroelastic analysis at this point gives actual values of F_v and F_p as 0.7250 and 0.5482, respectively. This is about 27% reduction in hub vibration and about 45% reduction in flap power from the initial design point. The design point A is a better design both in terms of hub vibration and trailing-edge flap power.

Best design point using response surface method: it can be seen that many good designs are obtained using the response surface approximation even though the second order polynomial fit is not good across the domain considered. The design point A ($x_1 = 0.65R$, $x_2 = 0.77R$, $GJ = 0.00461$) is the best design obtained by multi-objective optimization. This optimum design point gives about 27% reduction in hub vibration with about 45% reduction in flap control power.

2. Neural Network

Single objective optimization: at first, a single objective optimization is conducted using the neural network metamodel. An exhaustive search conducted in the design space using neural network as metamodel with the objective of minimizing the hub vibration alone gives $x_1 = 0.66R$, $x_2 = 0.89R$ and $GJ = 0.00461$ as the optimal point. Actual aeroelastic analysis at this point gives $F_v = 0.6135$ and $F_p = 1.0009$, which shows about 39% reduction in hub vibration with flap power being almost same as that of baseline value. A similar search with the objective of minimizing the trailing-edge flap power gives $x_1 = 0.59R$, $x_2 = 0.77R$ and $GJ = 0.00461$ as the optimal point with actual $F_v = 0.7589$ and $F_p = 0.5915$, showing a reduction of about 41% in flap power and about 24% reduction in hub vibration. The accurate nature of the neural network metamodel yields better results along expected lines for the single objective optimization.

The results show that the torsional stiffness, GJ should be at its lower move limit to achieve maximum reduction in both vibration and flap power. Outboard flap has to be placed at its upper move limit near the blade tip ($0.89R$) to achieve minimum vibration and it is to be placed at its lower move limit ($0.77R$) to minimize flap power.

Multi-objective optimization: because of the conflicting nature of this requirement, a "compromise design" which will minimize both

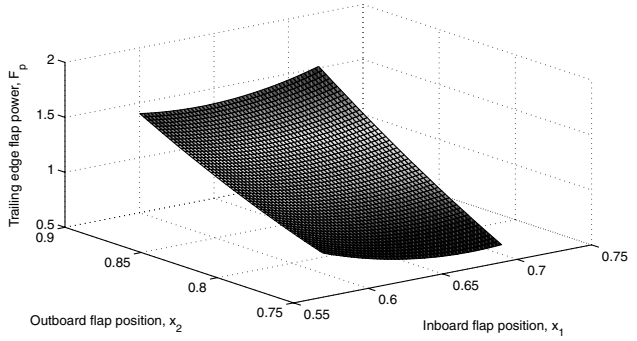

a) Response surface method

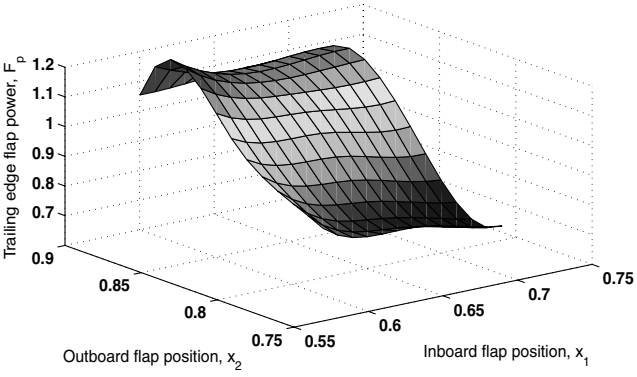

b) Aeroelastic analysis

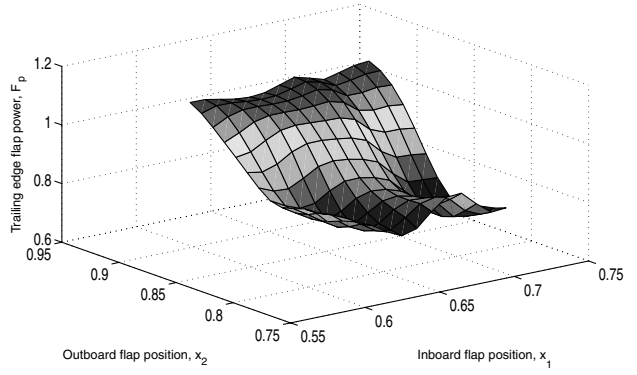

c) Neural network

Fig. 8 Variation in trailing-edge flap power, F_p, with respect to inboard flap position, x_1, and outboard flap position, x_2, with torsional stiffness, GJ, held constant at baseline value.

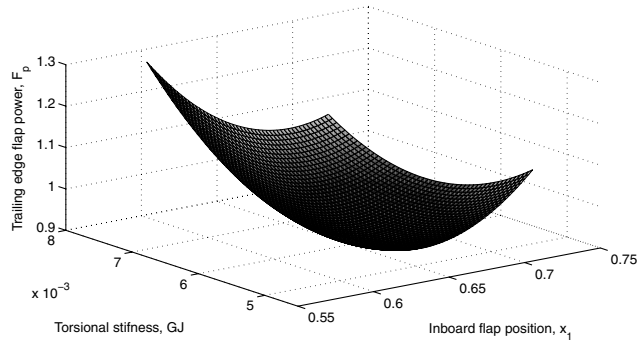

a) Response surface method

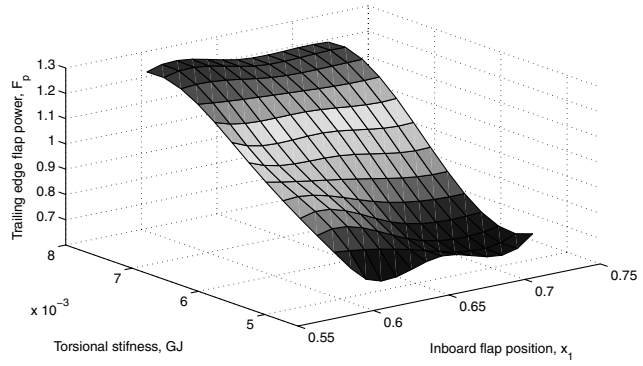

b) Aeroelastic analysis

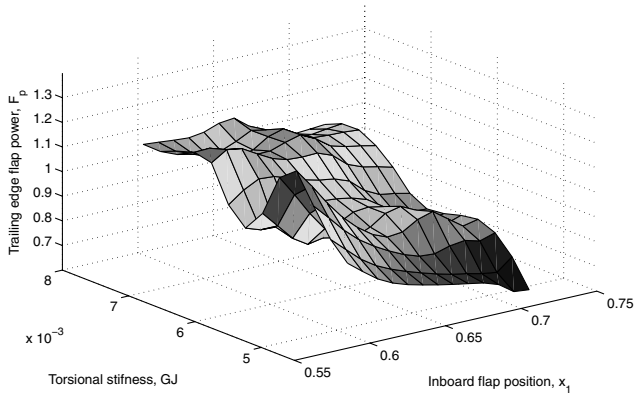

c) Neural network

Fig. 9 Variation in trailing-edge flap power, F_p, with respect to inboard flap position, x_1, and torsional stiffness, GJ, with outboard flap position, x_2, held constant at baseline value.

vibration levels and trailing-edge flap power compared with initial design is explored. Figure 12 shows the hub vibration levels and trailing-edge flap power resulting from various design choices within the move limits. It is obtained by moving from design space (x_1, x_2, GJ) to criterion space (F_v, F_p) using neural network metamodel. The design point $F_v = F_p = 1$ corresponds to the initial design point (baseline value). The initial design point and the Pareto surfaces are shown in Fig. 13.

In Fig. 13, curve BCD and curve EF represents globally and locally Pareto-optimal set, respectively, of this multi-objective optimization [53]. Design points B and D in Fig. 13 are the same optimum design points obtained by single objective optimization with the objective of minimizing F_v alone and F_p alone, respectively. Point C represents design point with $x_1 = 0.62R$, $x_2 = 0.77R$ and $GJ = 0.00461$. Aeroelastic analysis at this design point gives actual $F_v = 0.7319$ and $F_p = 0.5523$. This is about 27% reduction in hub vibration and about 45% reduction in trailing-edge flap power.

Point E on locally Pareto-optimal set in Fig. 13 corresponds to the design variables $x_1 = 0.60R$, $x_2 = 0.77R$ and $GJ = 0.00681$. Aeroelastic analysis gives actual $F_v = 0.9862$ and $F_p = 0.8266$ at this point. This is only about 17% reduction in flap power compared with initial design without much change in hub vibration from the initial design point. Similarly, point F represents the design point with $x_1 = 0.71R$, $x_2 = 0.77R$ and $GJ = 0.00769$. Actual $F_v = 1.1076$ and $F_p = 0.6404$ at this point. This gives about 36% reduction in flap power compared with initial design but at the cost of increasing hub vibration by about 11% compared with initial design. This shows that the design points E and F are not good design choices for this optimization problem. However, point E does provide the possibility of considerable reduction in flap power for a torsionally stiffer blade.

Best design point using neural network: design point B ($x_1 = 0.66R$, $x_2 = 0.89R$, $GJ = 0.00461$) gives about 39% reduction in hub vibration without much change in flap power requirement compared with initial design point. Design point C

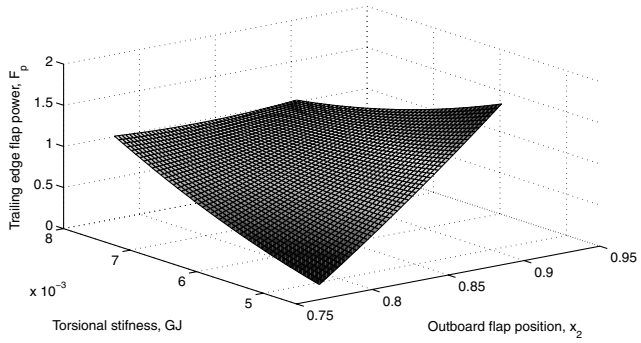

a) Response surface method

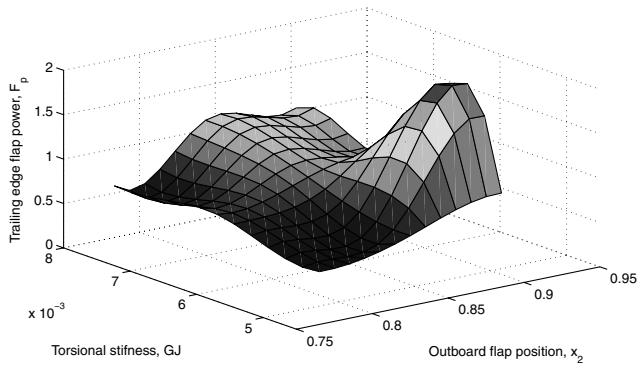

b) Aeroelastic analysis

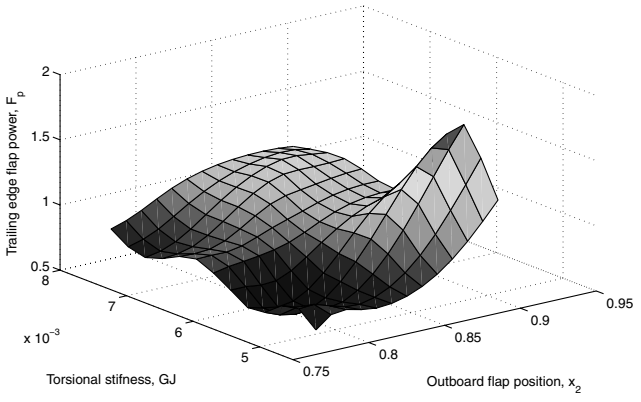

c) Neural network

Fig. 10 Variation trailing-edge flap power, F_p, with respect to outboard flap position, x_2, and torsional stiffness, GJ, with inboard flap position, x_1, held constant at baseline value.

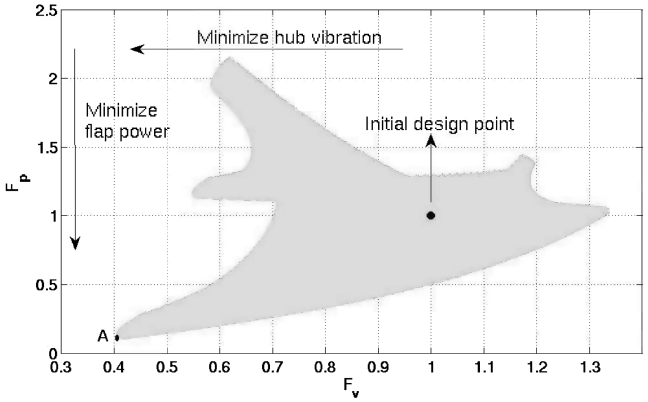

Fig. 11 F_v vs F_p for various design points within the move limits using response surface method.

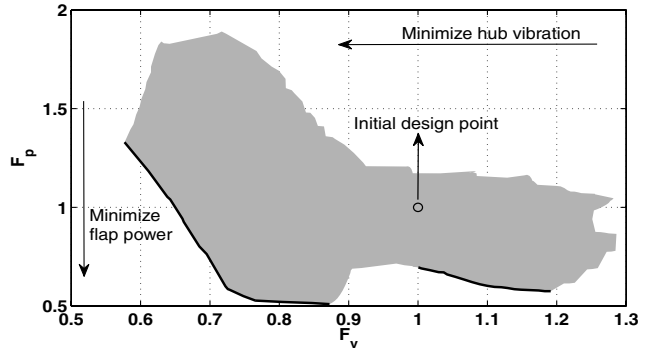

Fig. 12 F_v vs F_p for various design points within the move limits using neural network.

$(x_1 = 0.62R, x_2 = 0.77R, GJ = 0.00461)$ gives a reduction of about 27% in hub vibration and 45% in flap power. Design point D $(x_1 = 0.59R, x_2 = 0.77R, GJ = 0.00461)$ has about 41% reduction in flap power and about 24% reduction in hub vibration. This actual analysis results at design point D shows lesser reduction in both hub vibration and flap power objectives compared with that at design point C. Hence, design point D is not a good design choice. Design point B gives maximum reduction in hub vibration, but without much change in trailing-edge flap power from the initial design. Design point C gives considerable reduction in both hub vibration and trailing-edge flap control power and is probably the most useful design. There are many usable designs along the curve BCD in Fig. 13. The best design can be selected from the Pareto surface depending on the requirement in vibration reduction and constraints on the available flap control power.

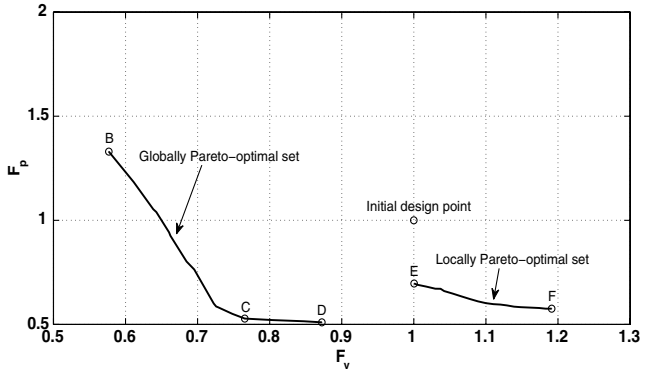

Fig. 13 Initial design point and globally and locally Pareto-optimal solutions using neural network.

Table 5 Comparison of design points obtained by response surface method and neural network using multi-objective optimization

	Design variables			Percent reduction in	
Design point	x_1	x_2	GJ	F_v	F_p
	Response surface method				
A	$0.65R$	$0.77R$	0.00461	27	45
	Neural network				
B	$0.66R$	$0.89R$	0.00461	39	0
C	$0.62R$	$0.77R$	0.00461	27	45
D	$0.59R$	$0.77R$	0.00461	24	41
E	$0.60R$	$0.77R$	0.00681	1	17
F	$0.71R$	$0.77R$	0.00769	−11	36

3. Comparison of Design Points Obtained by Response Surface Method and Neural Network

Table 5 gives a comparison of design points obtained by multi-objective optimization using response surface and neural network metamodels. Design point B obtained using neural network gives maximum reduction in hub vibration (39%) without much change in flap power from the initial design point. Design point A obtained using response surface method and design point C obtained using neural network gives almost same reduction in both hub vibration (27%) and flap power (45%) objectives. It is interesting to note that

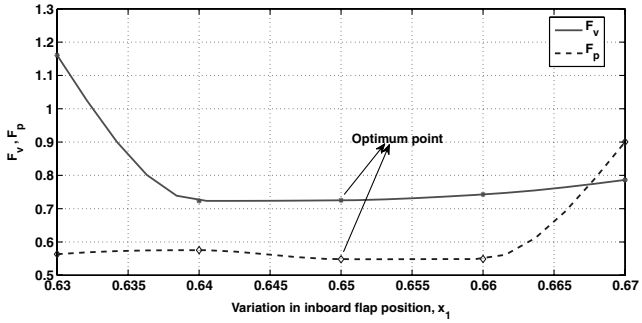

a) With inboard flap position, x_1

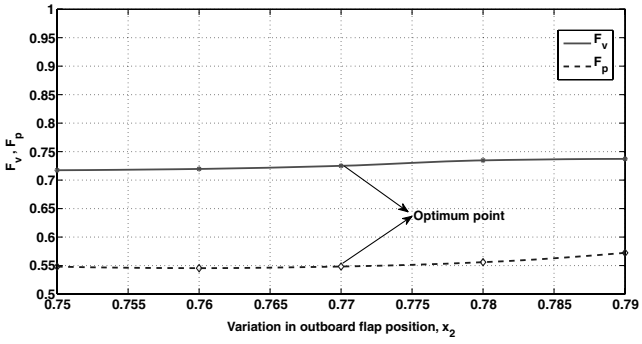

b) With outboard flap position, x_2

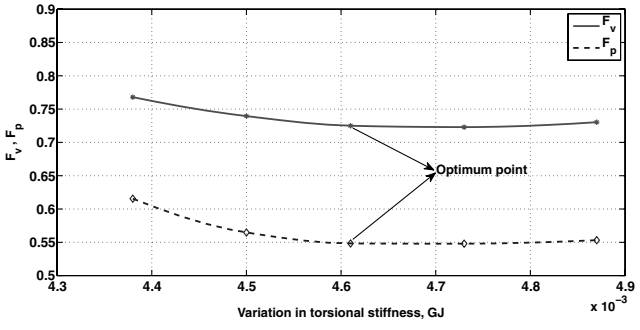

c) With blade torsional stiffness, GJ

Fig. 14 Sensitivity of optimum point obtained using RSM to changes in the design variables.

the response surface gives good results even though the flap power prediction is not accurate. However, the use of neural networks prevents anomalous results.

D. Sensitivity Analysis

1. RSM Optimum

Sensitivity of the optimum design point A ($x_1 = 0.65R$, $x_2 = 0.77R$, $GJ = 0.00461$) obtained using response surface method is checked by perturbing the design variables around the optimum design point. Figures 14a–14c show the variation of objective functions F_v and F_p with variations in design variables x_1, x_2 and GJ around the optimum point. In these cases, one design variable is changed and the other two are kept fixed and the results are obtained using aeroelastic analysis. It is found that the optimum design point obtained by RSM is less sensitive to small perturbations of the design variables. The movement of inboard flap further inwards from the optimum design point affects the hub vibration objective. Also the movement of inboard flap towards the tip from the optimum point increases flap power.

2. Neural Network Optimum

Similarly, sensitivity of the optimum design point C ($x_1 = 0.62R$, $x_2 = 0.77R$, $GJ = 0.00461$) obtained using neural network is also analyzed. Figures 15a–15c show the variation of objective functions F_v and F_p with variations in design variables x_1, x_2 and GJ around the optimum point. These results are also obtained using the aeroelastic analysis by varying one design variable around the optimum, keeping the other two fixed. It is found that the hub vibration, F_v is highly sensitive to the flap positions x_1 and x_2. Also, a small reduction in torsional stiffness, GJ from the optimum point increases both vibration and flap power. Movement of inboard flap towards the root adversely affects the flap power objective. Small perturbations of position of outboard flap around the optimum do not have much effect on trailing-edge flap power. The effect of perturbations of torsional stiffness on hub vibration is less compared with the position of the trailing-edge flaps. We see that the optimal point obtained using response surfaces is somewhat more robust compared with that obtained using the neural network.

Before concluding, we should point out that the metamodels are only used to guide the optimization process, to create criterion space and extract the Pareto points. The values of F_v and F_p for the different designs are obtained by running the analysis.

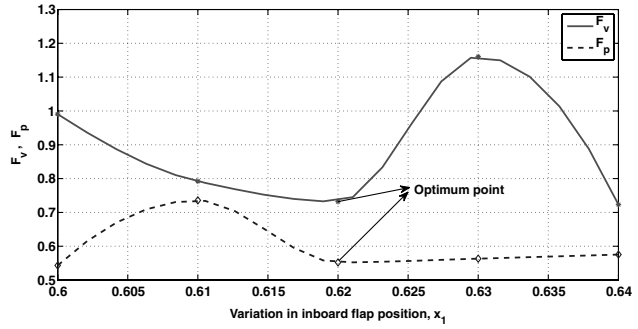

a) With inboard flap position, x_1

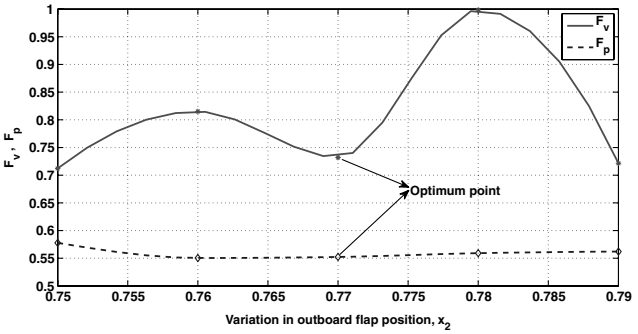

b) With outboard flap position, x_2

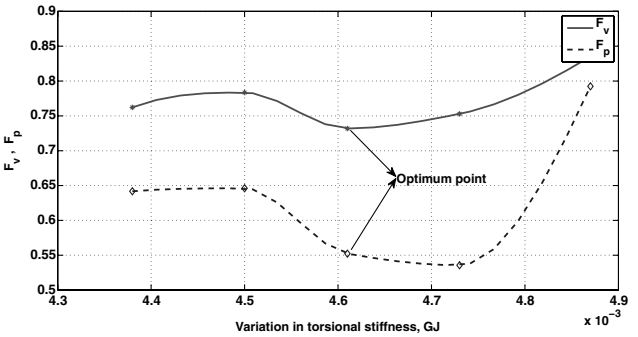

c) With blade torsional, GJ

Fig. 15 Sensitivity of optimum point obtained using neural network to changes in the design variables.

IX. Conclusions

Optimization results for the placement of dual trailing-edge flaps and torsional stiffness of the rotor blade are obtained for low hub vibration with minimum flap control power. Second order polynomial response function and neural network metamodels are used to approximate the objectives. These metamodels are used as a guide to reach the optimum of the problem. Aeroelastic analysis at these optimum design points gives actual reduction in hub vibration and flap power. The locations of the dual trailing-edge flaps and torsional stiffness of the rotor blade are the design variables and hub vibration level and required trailing-edge flap power are the objectives. The following conclusions can be made from this study.

1) Among the three stiffnesses (flap, lag and torsion), reduction in torsional stiffness contributes most favorably to the objectives of minimizing hub vibration and trailing-edge flap power. The inclusion of torsional stiffness as a design variable along with the location of the two trailing-edge flaps is found to be very beneficial for both of the objectives.

2) The introduction of torsional stiffness as a design variable makes the flap power objective function highly nonlinear. Polynomial response surface functions are unable to approximate these highly nonlinear functions adequately. Neural network metamodel is able to approximate these highly nonlinear functions fairly well compared with RSM.

3) Optimization in hub vibration and flap power with locations of dual trailing-edge flaps and torsional stiffness of the blade as design variables is done using response surface method and neural network metamodel and the results are compared. Some good designs are obtained using the response surface approximation even though the second order polynomial fit for flap power is not good across the domain considered. Pareto-optimal front minimizing both hub vibration and flap power are obtained using RSM and neural network metamodels for the multi-objective optimization.

4) An optimum design point A ($x_1 = 0.65R$, $x_2 = 0.77R$, $GJ = 0.00461$) obtained by response surface method gives about 27% reduction in hub vibration and about 45% reduction in flap power from the initial design point (baseline value). Similarly, the optimum design point C ($x_1 = 0.62R$, $x_2 = 0.77R$, $GJ = 0.00461$) obtained using neural network also gives almost same reduction in both the objectives. This shows that even though the response surface functions do not approximate the objective functions adequately, they are capable of guiding to better designs with considerable reduction in hub vibration and flap power objectives.

5) Torsional stiffness value goes to the lower move limit for the reduction of hub vibration and flap power. However, there exist torsionally stiffer blades which yield substantial flap power reduction.

6) Sensitivity of the optimum design points obtained by both RSM and neural network metamodels is analyzed. This analysis at the optimum design point C ($x_1 = 0.62R$, $x_2 = 0.77R$, $GJ = 0.00461$),

which is obtained by neural network metamodel shows that the hub vibration is quite sensitive to positions of the flaps compared with torsional stiffness of the rotor blade. But the flap power is more sensitive to torsional stiffness than the flap positions. The response surface based design shows less sensitivity to perturbations in design variables.

References

[1] Friedmann, P. P., "The Renaissance of Aeroelasticity and its Future," *Journal of Aircraft*, Vol. 36, No. 1, 1999, pp. 105–121. doi:10.2514/2.2418

[2] Loewy, R., "Helicopter Vibrations: A Technological Perspective," *Journal of the American Helicopter Society*, Vol. 29, No. 4, Oct. 1984, pp. 4–30. doi:10.4050/JAHS.29.4

[3] Nguyen, K., and Chopra, I., "Application of Higher Harmonic Control to Rotors Operating at High Speed and Maneuvering Flight," *Journal of the American Helicopter Society*, Vol. 35, No. 3, 1990, pp. 78–89. doi:10.4050/JAHS.35.78

[4] Hammond, C. E., "Wind Tunnel Results Showing Rotor Vibratory Loads Reduction Using Higher Harmonic Blade Pitch," *Journal of the American Helicopter Society*, Vol. 28, No. 1, 1983, pp. 10–15. doi:10.4050/JAHS.28.10

[5] Guinn, K. F., "Individual Blade Control Independent of a Swashplate," *Journal of the American Helicopter Society*, Vol. 27, No. 3, July 1982, pp. 25–31.

[6] Ham, N. D., "A Simple System for Helicopter Individual Blade Control Using Modal Decomposition," *Vertica*, Vol. 4, No. 1, 1980, pp. 23–28.

[7] Milgram, J., Chopra, I., and Straub, F. K., "Rotors with Trailing Edge Flap: Analysis and Comparison with Experimental Data," *Journal of the American Helicopter Society*, Vol. 43, No. 4, 1998, pp. 319–332. doi:10.4050/JAHS.43.319

[8] Friedmann, P. P., De Terlizzi, M., and Myrtle, T. F., "New Developments in Vibration Reduction with Actively Controlled Trailing Edge Flaps," *Mathematical and Computer Modelling*, Vol. 33, Nos. 10–11, 2001, pp. 1055–1083. doi:10.1016/S0895-7177(00)00300-9

[9] Fulton, M. V., and Ormiston, R. A., "Hover Testing of a Small Scale Rotor with On-Blade Elevons," *Journal of the American Helicopter Society*, Vol. 46, No. 2, 2001, pp. 96–106. doi:10.4050/JAHS.46.96

[10] Koratkar, N. A., and Chopra, I., "Wind Tunnel Testing of a Smart Rotor Model with Trailing-Edge Flaps," *Journal of the American Helicopter Society*, Vol. 47, No. 4, 2002, pp. 263–272. doi:10.4050/JAHS.47.263

[11] Viswamurthy, S. R., and Ganguli, R., "An Optimization Approach to Vibration Reduction in Helicopter Rotors with Multiple Active Trailing Edge Flaps," *Aerospace Science and Technology*, Vol. 8, No. 3, 2004, pp. 185–194. doi:10.1016/j.ast.2003.10.003

[12] Kim, J. S., Smith, E. C., and Wang, K. W., "Helicopter Vibration Suppression via Multiple Trailing Edge Flaps Controlled by Resonance Actuation System," American Helicopter Society 60th Annual Forum, Baltimore, MD, 7–10 June 2004.

[13] Chattopadhyay, A., "Vibration Reduction in an Articulated Rotor Blade Using Structural Optimization," *Engineering Optimization*, Vol. 19, No. 1, 1992, pp. 37–50. doi:10.1080/03052159208941219

[14] Ganguli, R., and Chopra, I., "Aeroelastic Optimization of a Helicopter Rotor to Reduce Vibration and Dynamic Stresses," *Journal of Aircraft*, Vol. 33, No. 4, 1996, pp. 808–815. doi:10.2514/3.47018

[15] Celi, R., and Friedmann, P. P., "Structural Optimization with Aeroelastic Constraints of Rotor Blades with Straight and Swept Tips," *AIAA Journal*, Vol. 28, No. 5, 1990, pp. 928–936. doi:10.2514/3.25141

[16] Venkatesan, C., Friedmann, P. P., and Yuan. K. A., "A New Sensitivity Analysis for Structural Optimization of Composite Rotor Blades," *Mathematical and Computer Modelling*, Vol. 19, Nos. 3–4, 1994, pp. 1–25. doi:10.1016/0895-7177(94)90054-X

[17] Yuan, K. A., and Friedmann, P. P., "Structural Optimization for Vibratory Loads Reduction of Composite Helicopter Rotor Blades with Advanced Geometry Tips," *Journal of the American Helicopter Society*, Vol. 43, No. 3, 1998, pp. 246–257. doi:10.4050/JAHS.43.246

[18] Ganguli, R., and Chopra, I., "Aeroelastic Optimization of an Advanced Geometry Helicopter Rotor," *Journal of the American Helicopter Society*, Vol. 41, No. 1, 1996, pp. 18–29. doi:10.4050/JAHS.41.18

[19] Gandhi, F., and Sekula, M. K., "Helicopter Vibration Reduction Using Fixed-System Auxiliary Moments," *AIAA Journal*, Vol. 42, No. 3, 2004, pp. 501–512. doi:10.2514/1.575

[20] Chattopadhyay, A., and McCarthy, T. R., "A Multidisciplinary Optimization Approach for Vibration Reduction in Helicopter Rotor Blades," *Computer and Mathematics with Applications*, Vol. 25, No. 2, 1993, pp. 59–72.

[21] Kim, J. E., and Sarigul-Klijn, N., "Elastic-Dynamic Rotor Blade Design with Multi-Objective Optimization," *AIAA Journal*, Vol. 39, No. 9, 2001, pp. 1652–1661. doi:10.2514/2.1512

[22] Soykasap, O., and Hodges, D. H., "Performance Enhancement of a Composite Tilt-Rotor Using Aeroelastic Tailoring," *Journal of Aircraft*, Vol. 37, No. 5, 2000, pp. 850–858. doi:10.2514/2.2680

[23] Murugan, S., Ganguli, R., and Harursampath, D., "Aeroelastic Analysis of Composite Helicopter Rotor with Random Material Properties," *AIAA Journal*, Vol. 45, No. 1, 2008, pp. 306–322.

[24] Ganguli, R., "Survey of Recent Developments in Rotorcraft Design Optimization," *Journal of Aircraft*, Vol. 41, No. 3, 2004, pp. 493–510. doi:10.2514/1.58

[25] Simpson, T. W., Peplinski, J. D., Koch, P. N., and Allen, J. K., "Metamodels for Computer-Based Engineering Design: Survey and Recommendations," *Engineering Computations*, Vol. 17, No. 2, 2001, pp. 129–150.

[26] Barthelemy, J. F. M., and Haftka, R. T., "Approximation Concepts for Optimum Structural Design: A Review," *Structural Optimization*, Vol. 5, No. 3, 1993, pp. 129–144. doi:10.1007/BF01743349

[27] Sobieszczanski-Sobieski, J., and Haftka, R. T., "Multidisciplinary Aerospace Design Optimization: Survey of Recent Developments," *Structural Optimization*, Vol. 14, No. 1, 1997, pp. 1–23. doi:10.1007/BF01197554

[28] Glaz, B., Friedmann, P. P., and Liu, L., "Helicopter Vibration Reduction Throughout the Entire Flight Envelope Using Surrogate-Based Optimization," *Journal of the American Helicopter Society*, Vol. 54, No. 1, 2009.

[29] Bhadra, S., and Ganguli, R., "Aeroelastic Optimization of a Helicopter Rotor Using Orthogonal Array-Based Metamodels," *AIAA Journal*, Vol. 44, No. 9, 2006, pp. 1941–1951. doi:10.2514/1.11776

[30] Myers, R. H., and Montgomery, D. C., *Response Surface Methodology: Process and Product Optimization Using Designed Experiments*, Wiley, New York, 1995.

[31] Agarwal, H., and Renaud, J. E., "Reliability Based Design Optimization Using Response Surfaces in Application to Multi-disciplinary Systems," *Engineering Optimization*, Vol. 36, No. 3, 2004, pp. 291–311. doi:10.1080/03052150410001666578

[32] Venkataraman, S., "Reliability Optimization Using Probabilistic Sufficiency Factor and Correction Response Surface," *Engineering Optimization*, Vol. 38, No. 6, 2006, pp. 671–685. doi:10.1080/03052150600711190

[33] Matheron, G., "Principles of Geostatics," *Economic Geology and the Bulletin of the Society of Economic Geologists*, Vol. 58, No. 8, 1963, pp. 1246–1266. doi:10.2113/gsecongeo.58.8.1246

[34] Glaz, B., Friedmann, P. P., and Liu, L., "Surrogate Based Optimization of Helicopter Rotor Blades for Vibration Reduction in Forward Flight," *Structural and Multidisciplinary Optimization*, Vol. 35, No. 4, 2008, pp. 341–363. doi:10.1007/s00158-007-0137-z

[35] Jin, R., Chen, W., and Simpson, T. W., "Comparative Studies of Metamodeling Techniques Under Multiple Modelling Criteria," *Structural and Multidisciplinary Optimization*, Vol. 23, No. 1, 2001, pp. 1–13. doi:10.1007/s00158-001-0160-4

[36] Ganguli, R., "Optimum Design of a Helicopter Rotor for Low Vibration Using Aeroelastic Analysis and Response Surface Methods," *Journal of Sound and Vibration*, Vol. 258, No. 2, 2002, pp. 327–344. doi:10.1006/jsvi.2002.5179

[37] Viswamurthy, S. R., and Ganguli, R., "Optimal Placement of Trailing-Edge flaps for Helicopter Vibration Reduction Using Response Surface

Methods," *Engineering Optimization*, Vol. 39, No. 2, March 2007, pp. 185–202.
doi:10.1080/03052150601047123

[38] Haykin, S., *Neural Networks: A Comprehensive Foundation*, 2nd ed., Prentice–Hall, Upper Saddle River, NJ, 1998.

[39] Hornik, K., Stinchcombe, M., and White, H., "Multilayer Feedforward Networks are Universal Approximators," *Neural Networks*, Vol. 2, No. 5, 1989, pp. 359–366.
doi:10.1016/0893-6080(89)90020-8

[40] Hornik, K., Stinchcombe, M., and White, H., "Universal Approximation of an Unknown Mapping and its Derivatives Using Multilayer Feedforward Networks," *Neural Networks*, Vol. 3, No. 5, 1990, pp. 551–560.
doi:10.1016/0893-6080(90)90005-6

[41] Hornik, K., "Approximation Capabilities of Multilayer Feedforward Networks," *Neural Networks*, Vol. 4, No. 2, 1991, pp. 251–257.
doi:10.1016/0893-6080(91)90009-T

[42] Lin, Z., Khorasani, K., and Patel, R. V., "A Counter-Propagation Neural Network for Function Approximation," *1990 IEEE International Conference on Systems, Man and Cybernetics Conference Proceedings*, 1990, pp. 382–384.

[43] Linse, D. J., and Stengel, R. F., "Neural Networks for Function Approximation in Nonlinear Control," *Proceedings of the 1990 American Control Conference*, Vol. 1, 1990, pp. 674–679.

[44] Lee, S. J., and Chen, H., "Design Optimization with Back-Propagation Neural Networks," *Journal of Intelligent Manufacturing*, Vol. 2, No. 5, 1991, pp. 293–303.
doi:10.1007/BF01471177

[45] Rumelhart, D. E., Widrow, B., and Lehr, M. A., "The Basic Ideas in Neural Networks," *Communications of the ACM*, Vol. 37, No. 3, 1994, pp. 87–92.
doi:10.1145/175247.175256

[46] Hajela, P., and Berke, L., "Neural Networks in Structural Analysis and Design: An Overview," *Computing Systems in Engineering*, Vol. 3, Nos. 1–4, 1992, pp. 525–538.
doi:10.1016/0956-0521(92)90138-9

[47] Lee, J., and Hajela, P., "Parallel Genetic Algorithm Implementation in Multidisciplinary Rotor Blade Design," *Journal of Aircraft*, Vol. 33, No. 5, 1996, pp. 962–969.
doi:10.2514/3.47042

[48] Zhang, J., Smith, E. C., and Wang, K. W., "Active-Passive Hybrid Optimization of Rotor Blades with Trailing Edge Flaps," *Journal of the American Helicopter Society*, Vol. 49, No. 1, 2004, pp. 54–65.
doi:10.4050/JAHS.49.54

[49] Leishman, J. G., "Indicial Lift Approximations for Two-Dimensional Subsonic Flow as Obtained from Oscillatory Measurements," *Journal of Aircraft*, Vol. 30, No. 3, 1993, pp. 340–351.
doi:10.2514/3.46340

[50] Hariharan, N., and Leishman, J. G., "Unsteady Aerodynamics of a Flapped Airfoil in Subsonic Flow by Indicial Concepts," *Journal of Aircraft*, Vol. 33, No. 5, 1996, pp. 855–868.
doi:10.2514/3.47028

[51] Bir, G., Chopra, I., and Ganguli, R., "University of Maryland Advanced Rotorcraft Code (UMARC) Theory Manual," : Univ. of Maryland, Dept. of Aerospace Engineering Rept. 92-02, 1992.

[52] Johnson, W., "Self-tTuning Regulators for Multicyclic Control of Helicopter Vibration," NASA TP 1996, March 1982.

[53] Deb, K., *Multi-Objective Optimization Using Evolutionary Algorithms*, John Wiley, Chichester, England, U.K., 2001.